Geophys. J. Int. (2003) **152,** 597–612

Determination of shallow shear wave velocity profiles in the Cologne, Germany area using ambient vibrations

Frank Scherbaum,[1] Klaus-G. Hinzen[2] and Matthias Ohrnberger[1]

[1] *Institut für Geowissenschaften der Universität Potsdam,* POB 601553, D-14415 *Potsdam, Germany. E-mail: fs@geo.uni-potsdam.de*
[2] *Abt. für Erdbebengeologie der Universität zu Köln, Vinzenz-Palotti-Str.* 26, D-51429 *Bergisch Gladbach, Germany*

Accepted 2002 August 29. Received 2002 August 21; in original form 2002 April 29

SUMMARY

We have used both single-station and array methods to determine shallow shear velocity site profiles in the vicinity of the city of Cologne, Germany from ambient vibration records. Based on *fk*-analysis we assume that fundamental-mode Rayleigh waves dominate the analysed wavefield in the frequency range of 0.7–2.2 Hz. According to this view a close relation exists between H/V spectral ratios and the ellipticity of the contributing Rayleigh waves. The inversion of the shape of H/V spectral ratios then provides quantitative information concerning the local shear wave velocity structure. However, based on tests with synthetic data believed to represent a typical situation in the Lower Rhine Embayment, dispersion curves were found to provide stronger constraints on the absolute values of the velocity–depth model than the ellipticities. The shape of the ellipticities was found to be subject to a strong trade-off between the layer thickness and the average layer velocity. We have made use of this observation by combining the inversion schemes for dispersion curves and ellipticities such that the velocity–depth dependence is essentially constrained by the dispersion curves while the layer thickness is constrained by the ellipticities. In order to test this method in practice, we have used array recordings of ambient vibrations from three sites where the subsurface geology is fairly well known and geotechnical information is at least partially available. In order to keep the parameter space as simple as possible we attempted to fit only a single layer over a half-space model. However, owing to earlier studies from the region, we assume a power-law depth dependence for sediment velocities. For all three sites investigated, the inversion resulted in models for which the shear wave velocity within the sediment layer both in absolute value at the surface and in depth dependence are found to be remarkably similar to the results obtained by Budny from downhole measurements. This is strong support for the interpretation of H/V spectral ratios as Rayleigh wave ellipticities. For all three sites the predicted *SH*-wave site amplification factors at the fundamental frequency are of the order of 5–6 with a slightly smaller value south of Cologne.

Key words: ambient vibrations, array measurements, shear wave velocity profile, site effects.

1 INTRODUCTION

Seismic risk in Germany is caused by the combination of moderate seismic hazard and high vulnerability in regions of high population density and concentration of industrial facilities. The Cologne area in NW Germany is a prime example of such a situation. Adding to the shakeability in this region is the fact that the shallow subsurface structure consists mostly of soft sediments overlying much stiffer layers, thus producing significant frequency-dependent soil amplifications. The distribution of shear wave velocities in these sediments is the key parameter for evaluating these effects (e.g. ESG98 1998). In this context, the analysis of ambient vibrations has gained considerable attention especially in Japan as a low cost tool for retrieving the shallow shear wave velocity structure quantitatively (Horike 1985; Tokimatsu *et al.* 1992; for reviews see Kudo 1995; Tokimatsu 1997; Bard 1998). These methods are now generally based on the assumption that ambient vibrations are dominated by surface waves. Single-station methods and array methods for determining site response properties from ambient vibrations are currently in use. Among the single-station methods, the H/V spectral ratio is most popular. Here, the ratios of spectral amplitudes of horizontal and vertical components are calculated. These spectral ratios often exhibit a distinct peak that is often empirically found to coincide with the fundamental quarter-wavelength 'resonance frequency' of the transmission response (Mooney & Bolt 1966; Lachet & Bard 1994; Tokimatsu 1997). However, if ambient

vibrations consist mostly of surface waves, the relationship between the body wave resonance and spectral ratio peak frequencies is not straightforward. In sedimentary basins with a strong impedance contrast between the soft sediments and the underlying bedrock, such a relationship might not exist (Al Yuncha & Luzón 2000). On the other hand, in simple 1D situations spectral ratios have more to offer than resonance frequencies. In this case, the average H/V spectral ratios can be assumed to measure the ellipticity of Rayleigh waves at the surface of a layered medium. Hence, the shape of the H/V spectral ratios can be used to determine the shear wave velocity profile (e.g. Arai & Tokimatsu 1998; Ishida *et al.* 1998; Miyakoshi *et al.* 1998; Fäh *et al.* 2001). In contrast to single-station methods, array methods make use of the dispersive properties of surface waves in layered media. Mostly vibrations measured using the vertical component are analysed in practice since they can rather safely be assumed to be dominated by Rayleigh waves. In this way, shear wave velocity profiles down to depths of several hundred metres have been obtained by inversion of dispersion curves of long-period surface waves (Horike 1985; Ishida *et al.* 1998; Miyakoshi *et al.* 1998; Yamamoto 1998). In this paper we employ both single-station and array methods to determine shallow site profiles in the Cologne area. One aspect of this paper is to determine whether both techniques provide independent information towards a unique structural model (Boore & Toksöz 1969). The main purpose, however, is to determine the degree of constraint that ambient vibrations provide on the prediction of frequency-dependent soil amplification in the Cologne area.

2 DATA SET

The city of Cologne, with a population close to 1 million, is located near the southeastern end of the Lower Rhine Embayment (LRE) in NW Germany, which is one of the most active seismic regions in Central Europe (Fig. 1). The shallow subsurface structure consists of soft Quaternary and Tertiary sediments overlaying Devonian shales and sandstones, which outcrop to the northeast and southwest. At three sites in the vicinity of the city, arrays were located near Pulheim, Chorweiler and Lülsdorf, respectively (Fig. 2). Each array (with an aperture of roughly 1 km) consisted of 13 elements, which were equipped with Lennartz LE5D three-component seismometers with an eigenperiod of 5 s. Owing to access constraints, the arrays were operated as cross arrays following local dirt roads and/or small trails. At each array location several hours of ambient vibrations were recorded using a sampling frequency of 125 Hz. The data were subsequently visually controlled to exclude obvious transient disturbances from nearby sources (e.g. passing

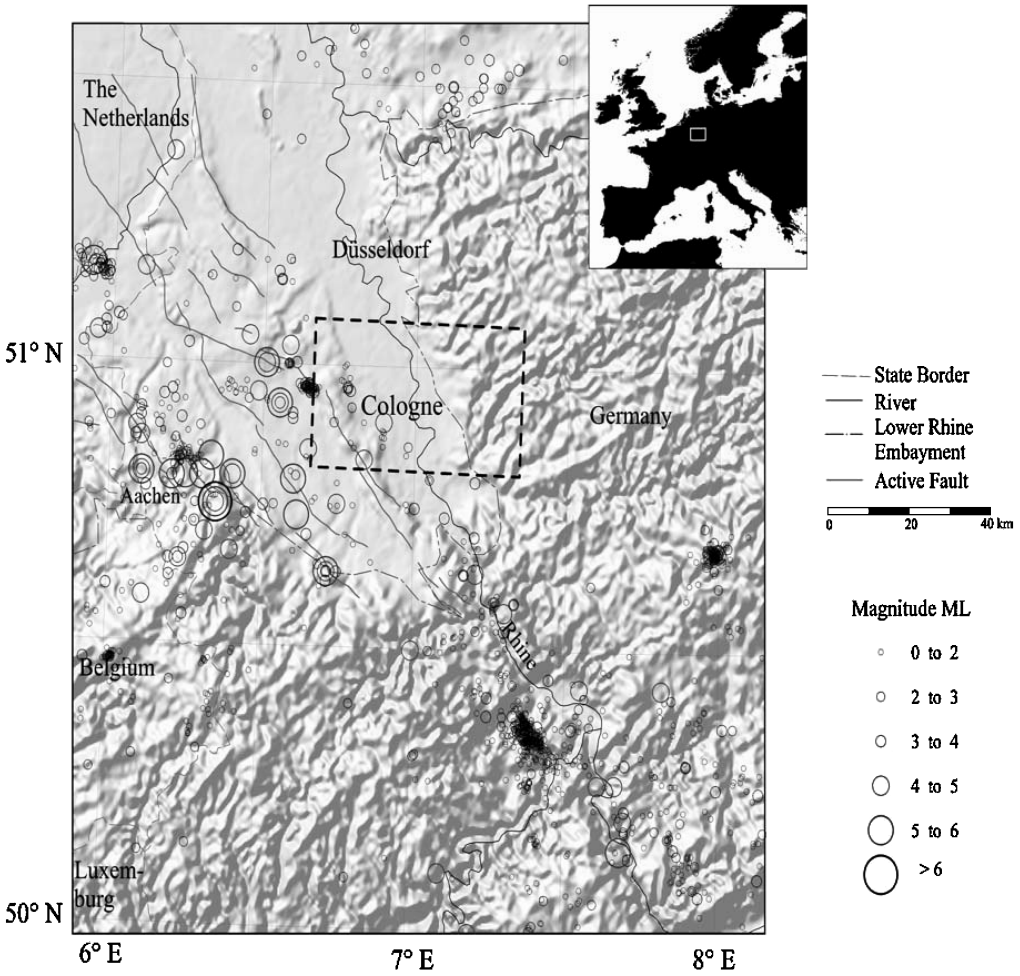

Figure 1. Historical seismicity in the Lower Rhine Embayment since 1000 AD and instrumentally recorded seismicity between 1950 and 1995 from the earthquake catalogue of the seismological station Bensberg plotted as circles. The larger earthquakes are concentrated on the western border faults of the Rur Graben system. The dashed square outlines the location of the simplified geological map in Fig. 2. DEM based on US Geological Survey (1993).

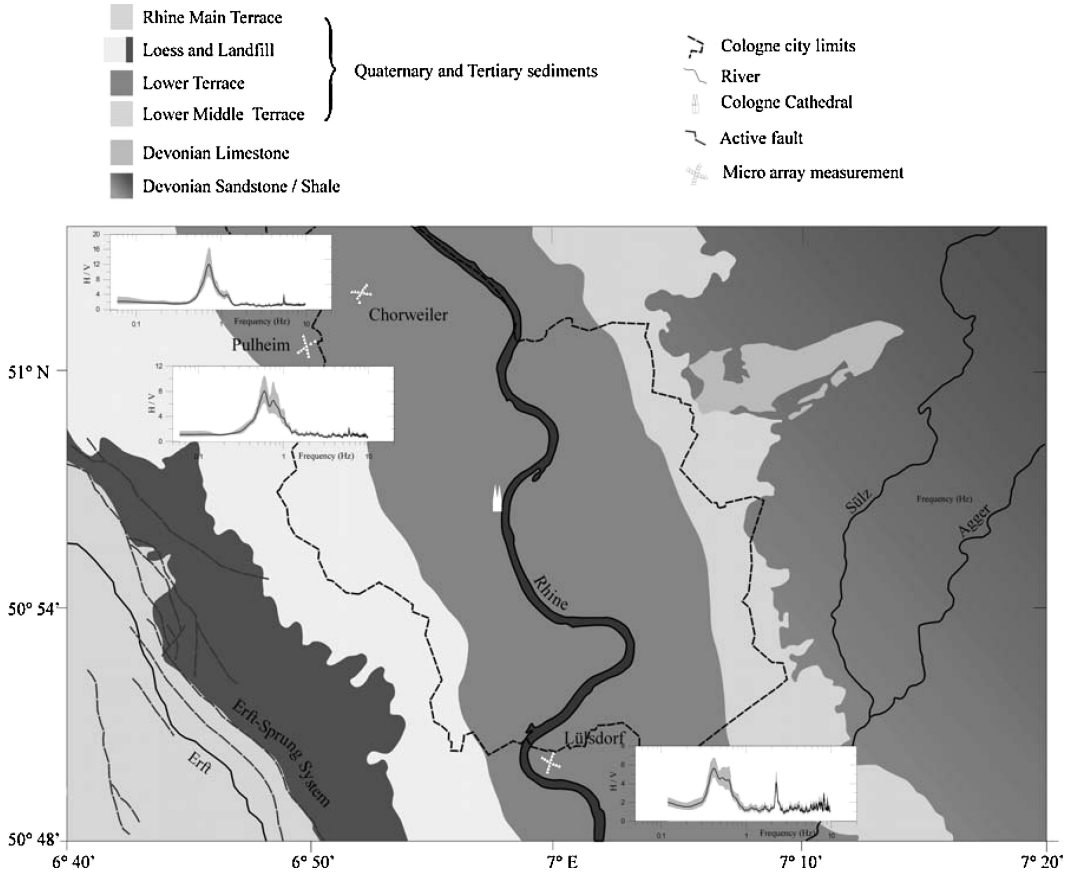

Figure 2. Array locations and simplified geological map of the study area.

vehicles, people walking nearby and cows). For the calculation of the H/V ratios, time windows of 15 min were selected for each of the sensor sites. Spectra for the horizontal and vertical components were calculated from running averages of time windows with 60 s length and an overlap of 30 s. H/V spectra for the central array locations are shown as insets on the map in Fig. 2 (log–linear scale). Table 1 (see Section 3.1) lists the averages and standard deviations for peak frequencies from all 13 measuring locations at each array site.

After visual quality control, dispersion curves were calculated for each array and selected time windows using a semblance-based *fk*-analysis. In order to determine the robustness of the results, three stacking techniques for the *fk*-grids were applied to the same data window. In the first approach, *fk*-spectra were stacked for different time windows before the phase velocity was determined, while in the second approach the maxima of individual *fk*-spectra were averaged for different time windows. In a third approach, only time windows for which the maximum coherence between all array traces falls within the range of the best 20 per cent were analysed with the same techniques. Above 1 Hz all the techniques essentially yield the same dispersion curves while at lower frequencies the results differ. The resulting scatter was quantified as a standard deviation from the sample mean and for the purpose of fitting theoretical dispersion curves used as frequency-dependent weighting factors. The resulting average dispersion curves and the resulting scatter (shown as error bars) are displayed in Fig. 3. Stable dispersion curves could be determined for frequencies from 0.7 up to 2.2 Hz. For the following considerations we assume that the fundamental modes of Rayleigh waves dominate the analysed wavefield, at least in the frequency range for which clear dispersion is observed. We searched for higher-mode contributions by azimuthally stacking the *fk*-spectral values along circles of constant phase velocities. If several modes were present, the resulting stacks should show multiple maxima as a function of phase velocity. However, the data consistently show only one single maximum, which leads us to the conclusion that fundamental-mode Rayleigh waves dominate the vertical component wavefield in our data set.

3 DETERMINATION OF THE SHEAR VELOCITY PROFILE

Since the dispersion curve and the ellipticity of Rayleigh waves are both controlled by the subsurface velocity structure, in principle we can invert either of them for shear wave velocity models (e.g. Tokimatsu 1997; Ishida *et al.* 1998). This is done by minimizing the misfit between the observed and the theoretical dispersion curve and/or ellipticity for simplified plane layered models. Since the resulting models are not unique, however, special care has to be taken regarding the parametrization (especially since we intend to use the models to estimate local site amplifications). The common approach to searching for the simplest model in terms of the numbers of layers that explains the observed dispersion curve and/or ellipticity, may produce models that overestimate site amplifications by introducing artificial impedance contrasts. Here, overestimation does not even mean conservatism in terms of site amplification since the peak frequencies might be off, resulting in an underestimation of site amplification at the true resonance frequencies. On the other hand,

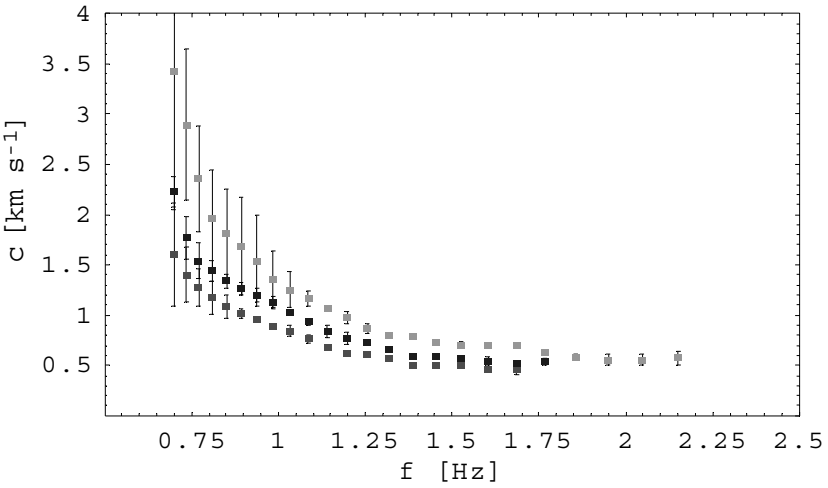

Figure 3. Dispersion curves obtained at the three array locations. Shown from top to bottom are the dispersion curves for Chorweiler, Pulheim, and Lülsdorf, respectively. The error bars do not represent the true uncertainty but the scatter resulting from the application of different stacking techniques.

overly smooth models are also inappropriate if the smoothness is just a consequence of lack of data resolution (e.g. frequency band limitation). This would result in an undesired underestimation of local site amplifications. Considering this dilemma, our strategy is to abandon the quest for a single best model serving all needs. Instead we attempt to find a set of good models that fit all the data adequately. To make this computationally feasible we reduce the model space to models with a single sedimentary unit over a half-space. For this unit we allow for a power-law depth dependence of the elastic parameters. For sedimentary rocks this seems to be a justifiable simplification, which includes a single homogeneous layer (if the exponent approaches zero) and a smooth gradient model (if the unit thickness increases) as end members of a fairly simple model set. For the study area *P*- and *S*-wave velocities and attenuation properties were experimentally determined at 32 sites in the Lower Rhine Embayment using seismic downhole measurements (Budny 1984). The resulting generalized relationships between dynamic soil properties and depth clearly support the assumption of a power-law depth dependence for compressional and shear wave velocities in the sedimentary coverage of the study area.

Another important practical aspect is the question of how one should combine models obtained from dispersion curves and H/V spectral ratios. Do dispersion curves and spectral ratios of ambient vibrations provide independent information leading to a unique site model? Are they sensitive to the same model features and how should the information be weighted relative to each other? Since answers to these questions may differ for different site classes we first test the performance of site structure inversion for a generic site model closely resembling the site conditions in the study area. In terms of the site characterization scheme to be adopted in the new German earthquake code (DIN4149new), the area under investigation would be characterized as subsoil class C (deep basin). Following a preparatory study for the new code by Brüstle & Stange (1999) we use their average model C with soil type 3 as a generic reference model.

3.1 Reference model for the Lower Rhine Embayment

Following the classification within the new German earthquake code, the deep basin model is characterized by a shallow (20 m) soil layer with constant geotechnical parameters. This is followed by a subsoil soft sedimentary unit with increasing shear wave velocities from 350 m s^{-1} at 20 m down to 800 m s^{-1} at a depth of 320 m where the shear velocity is assumed to jump to 1600 m s^{-1}, which is representative of consolidated Permo-Mesozoic sediments. Below this depth, *S*-wave velocities are assumed to increase further with depth down to a reference bedrock depth of 1 km. Here a first-order velocity discontinuity is assumed. The half-space velocity is 3300 m s^{-1}. The uppermost panel in Fig. 4 shows (a) the shear wave velocity profile for the generic deep basin model and (b) the corresponding *SH*-wave transfer function (top of half-space to surface) corrected for the free surface. The fundamental resonance appears close to 0.5 Hz, which is in good agreement with the observed H/V peak frequencies for the study area (Table 1). To test the sensitivity of the *SH*-wave site amplification function to details of the model, a set of modified models was generated (Fig. 4c). For this purpose layer thicknesses and geotechnical parameters of the reference model were randomly selected from truncated normal distributions centred around the given mean values. Variabilities and truncation limits were chosen to represent conceivable variations for the Lower Rhine Embayment. Fig. 4(d) shows the mean values and the standard deviation of the corresponding *SH*-wave site amplification functions. The latter scatter more or less symmetrically around the site amplification derived from the mean model (Fig. 4b) for the fundamental resonance peak, while for higher frequencies this is no longer the case (Fig. 4e). The individual model Fig. 4(a) is therefore believed to be a fair representation of a typical deep basin situation regarding the fundamental resonance peak.

3.1.1 Usable frequency range

The quality of shear wave velocity profiles determined from surface waves depends crucially on the frequency range in which dispersion curve and spectral ratios (ellipticities) are suitable for the inversion. The information concerning the deep parts of the model is contained in the low-frequency range while the shallow part is constrained by the information on the high-frequency part of the wavefield. The performance of an array to determine phase velocities is strongly dependent on the ratio of the array aperture (a) and the wavelength (λ). Decreasing a/λ, the array eventually loses its resolution to detect signal delays, which are the basis for the determination of phase

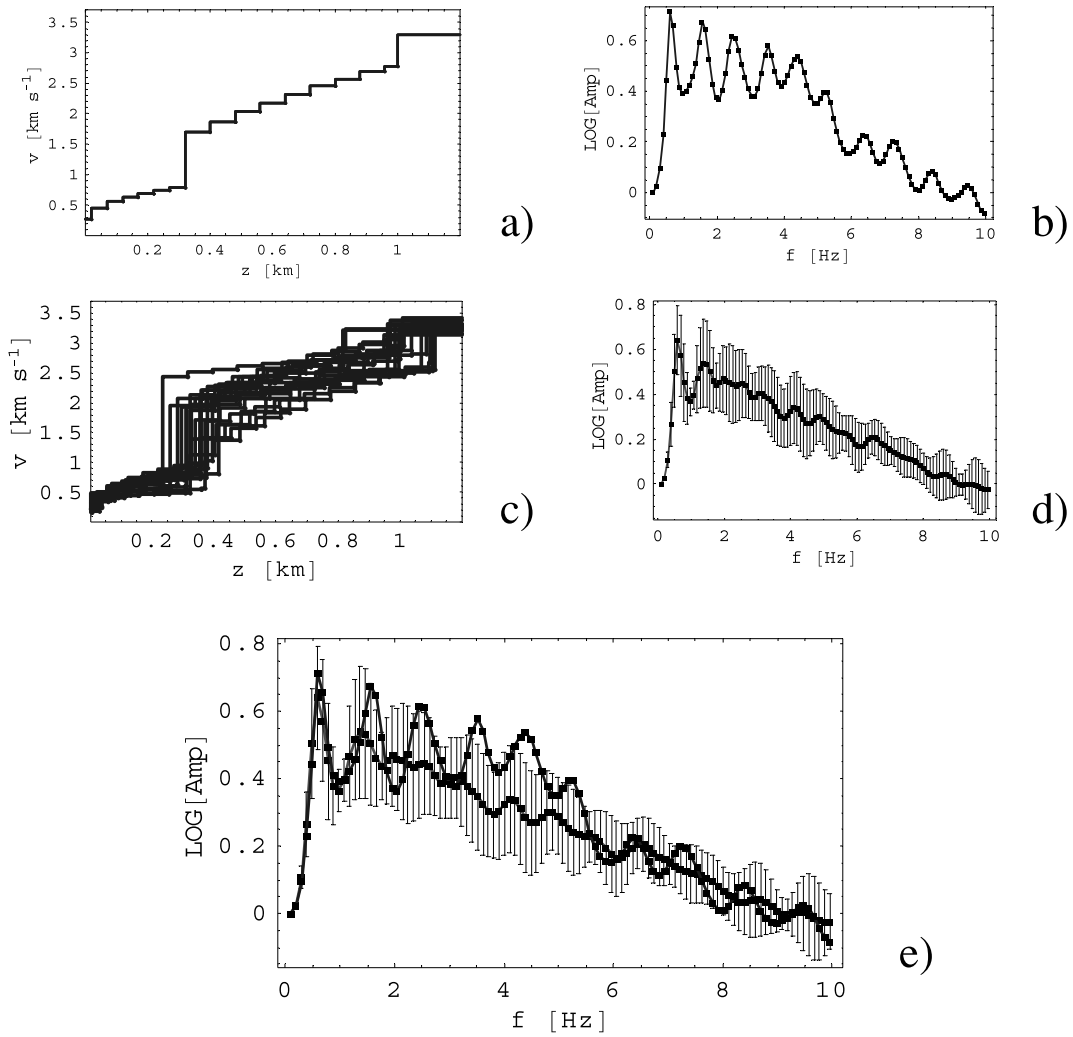

Figure 4. Reference basin model for the Lower Rhine Embayment and corresponding site amplification functions for plane *SH* waves: (a) mean model, (b) mean site amplification function, (c) randomized basin models and (d) corresponding site amplification functions, (e) superposition of (b) and (d).

Table 1. Average peak frequencies (Hz) of H/V spectra at array locations in the Cologne area. Single standard deviations from the measurements at the 13 array elements are given.

Array	NS/V	EW/V
Lülsdorf	0.38 ± 0.09	0.40 ± 0.02
Chorweiler	0.70 ± 0.02	0.71 ± 0.04
Pulheim	0.59 ± 0.02	0.59 ± 0.03

velocities. There is no firm rule as to where this occurs since it depends strongly on the noise conditions. Regarding the stability of H/V spectral ratios, Fäh *et al.* (2001) noted that for frequencies outside the range between the maximum and minimum of the ellipticity of Rayleigh waves these values become fairly sensitive to source distance effects. Consequently, for their inversion scheme they restrict the usable frequency range to the band between the maximum and the minimum ellipticity. Another aspect, however, is often neglected. A layered medium itself acts as a filter limiting the usable frequency range as well. To illustrate this point, we consider a single impulsive force acting obliquely to the surface of the reference model so that both Love and Rayleigh waves are generated. The (velocity proportional) amplitude spectrum for the resulting vertical and radial component seismograms (Fig. 5a) demonstrates the filter effects of the model on the different wave types and components. For Love waves this effect has been discussed theoretically in detail by Tazime (1957). For practical reasons, however, only vertical component records are used for the array analysis of ambient vibrations. Here, the frequency band limitation becomes especially severe at those frequencies where the amplitude of the vertical components vanishes, in other words close to the frequency of the maximum H/V spectral ratio. This is demonstrated in Fig. 5(b) which shows the dispersion curve for the reference model colour coded by the excitation strength of the vertical component of the Green function. The low-frequency limit for the determination of dispersion curves from vertical component records for a broad-band source correlates very well with the lowest frequency for which we were able to determine stable dispersion curves for the study area (roughly 0.7 Hz, *cf.* Fig. 3). Furthermore, the amplitude level of ambient vibrations in the low-frequency range is also known to be dependent on the meteorological conditions. Vertical ground motion excitation at frequencies below 0.5 Hz has been observed to be considerably increased under unstable weather conditions (Kudo 2002, *pers. comm.*). This raises the question of which of the factors (1) array aperture, (2) high pass

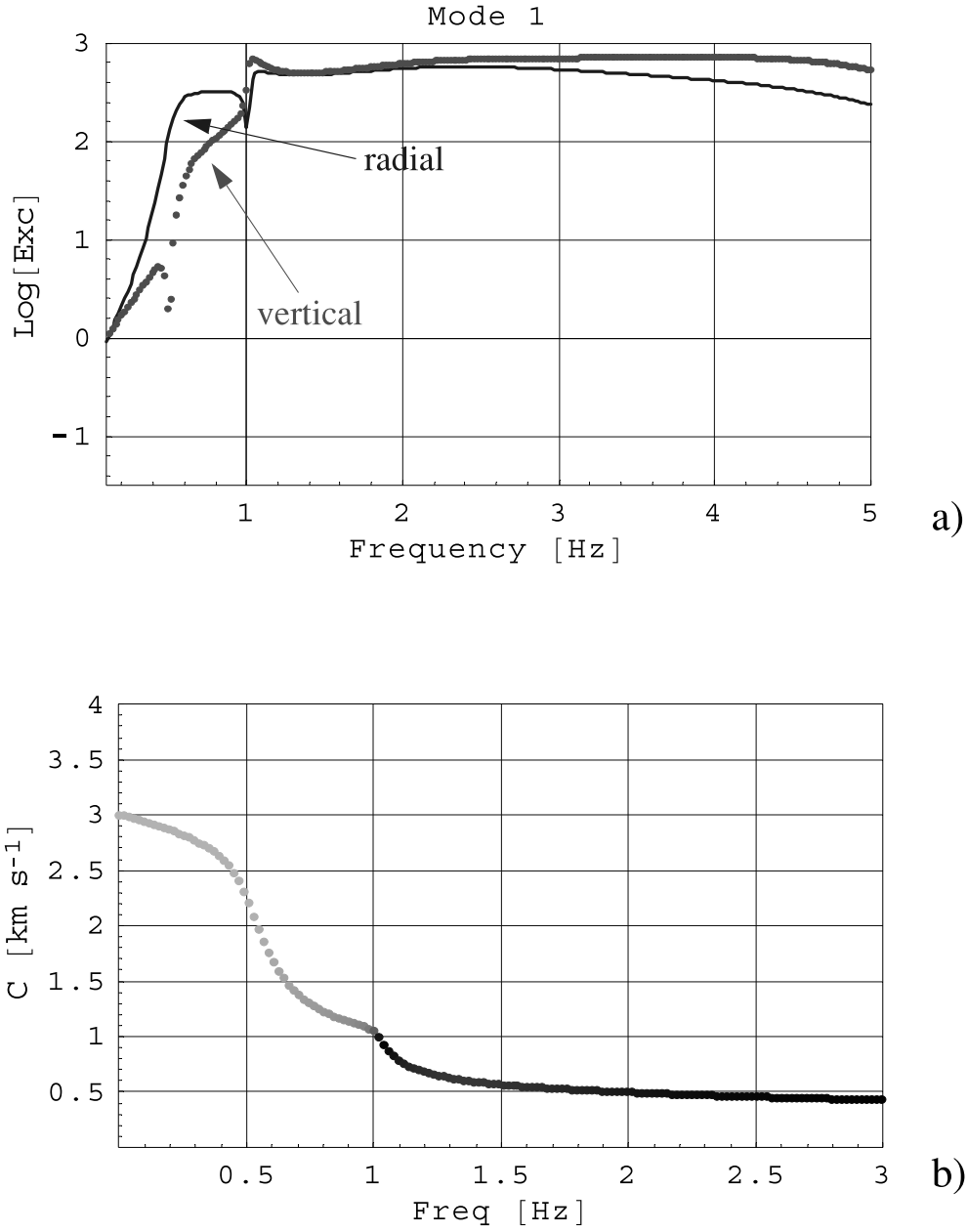

Figure 5. (a) Excitation function (proportional to ground velocity) for the radial and vertical component of a single impulsive force acting obliquely to the surface of the reference model, (b) dispersion curve for the reference model grey-shaded by the vertical excitation strength.

filter effect of the medium, (3) source excitation strength has more influence on the depth resolution of the shear wave velocity models obtained from dispersion curve inversion. This is the topic of an ongoing study.

A similar phenomenon applies to the determination of shear wave velocity profiles from spectral ratios. Spectral ratios are distorted by contributions of unmodelled wave types (Love waves on the horizontal component and body waves on all components) in the frequency ranges where there is no energy either on the horizontal or vertical component. To overcome this problem, we are currently testing an approach to separate Love and Rayleigh wave components of ambient vibrations by combined array and polarization processing based on the method of Ohrnberger (2001) but a further discussion is beyond the scope of this paper.

3.1.2 Misfit functions

To evaluate shear wave velocity models regarding their performance to explain the observed data we calculate a number of different cost functions. For the dispersion curve we use r_c defined as

$$r_c = \sqrt{\left(\sum_{i=1}^{N} \frac{[c_{obs}(f_i) - c_{theo}(f_i)]^2}{\sigma_c(f_i)^2} \right) \Big/ N} \qquad (1)$$

to quantify the misfit between N phase velocity values $c_{obs}(f_i)$ at observed frequencies f_i and the corresponding theoretical values $c_{theo}(f_i)$ calculated for the model under consideration. Since $\sigma_c(f_i)$ characterizes the uncertainty of the observation at frequency f_i, r_c, calculates the normalized deviation of the observed dispersion curve

from the model dispersion curve. A model dispersion curve that follows the upper or lower limit of the 'error bars' ($c_{\rm theo}(f_i) = c_{\rm obs}(f_i) \pm \sigma_{\rm c}(f_i)$) would result in a value of $r_{\rm c} = 1$. A similar expression $r_{\rm ell}$ is evaluated for the misfit between the shape of observed and theoretical ellipticities. The latter are calculated including a variable fraction of Love wave energy on the horizontal component.

In order to quantify how well a model is able to predict the extreme values of spectral ratios, three additional cost functions are defined. The deviations for the extrema of the observed spectral ratios and the corresponding model ellipticities are measured by $r_{\rm ellmax} = \sqrt{(f_{\rm maxHV} - f_{\rm maxEll})^2/\sigma^2_{\rm maxHV}}$ and $r_{\rm ellmin} = \sqrt{(f_{\rm minHV} - f_{\rm minEll})^2/\sigma^2_{\rm minHV}}$, respectively. Finally, $r_{\rm ellextr} = (r_{\rm ellmax} + r_{\rm ellmin})/2$ measures the joint misfit of the model ellipticities to explain both extreme values of the H/V spectral ratios.

Since we are dealing with relatively small model parameter sets, an exhaustive search of the model space is computationally quite feasible. This offers the advantage that the topology of the set of misfit values can be investigated in detail to check for intrinsic tradeoffs between model parameters. All the forward calculations were performed by modal summation using the code generously provided by R. B. Herrmann (1996).

3.1.3 Inversion results for the Lower Rhine Embayment reference model

In order to test the resolution of the models for the study area, we tried to reconstruct the reference model (Fig. 4a) from the frequency band-limited synthetic dispersion curve and spectral ratios. In accordance with the observations (Fig. 3), but also based on the considerations regarding the filter effects of a layered medium, we use 0.7 Hz as a low-frequency limit and 2.2 Hz as a high-frequency limit for the inversion. The corresponding model dispersion curve and ellipticity are shown in Figs 6 and 7, show the resulting shear wave velocity models together with the corresponding dispersion curves and ellipticities. The left-hand panels were obtained from the dispersion curve inversion, while the right-hand panels were obtained from the ellipticity inversion. Since the model that is used to fit the reference data (Fig. 6) consists only of a single layer over half-space (although with a power-law depth dependence), what we can hope to recover from the reference model at best is the shallow part. Fig. 7 shows that the dispersion curve and ellipticity inversion perform quite differently in this respect. From the band-limited inversion of the dispersion curve (left panels) the velocity profile for the uppermost 200–300 m is well recovered. The depths to the first strong impedance contrast in the 20 best-fitting models scatter roughly within 100 m. All the resulting model dispersion curves match the reference dispersion curve well within the frequency band used for the fit while outside this range the curves diverge drastically. This corresponds to the fact that as expected there is nearly no resolution for the half-space velocity. For models obtained from the ellipticity fit (right-hand panels) the velocity–depth profile is less well recovered (uppermost right-hand panel) even for the shallow portion. In addition to the scatter of the depths to the first strong impedance contrast, which is of the same order as for the dispersion curve fit, the velocities are also off considerably. In contrast to the dispersion curve, the shape of the ellipticity obviously does not constrain the absolute values of the velocity model. This can also be seen in the mismatch of the resulting dispersion curves with respect to the reference dispersion curve (second panel from the top). Regarding the half-space velocities the scatter is comparable to the results obtained from the dispersion curve inversion.

3.1.4 Sensitivity of ellipticity and phase velocity regarding layer structure

Judging from the results in Fig. 7, the dispersion curve seems to contain more recoverable information concerning the velocity structure than the shape of the ellipticities. This seems to be in conflict with the result of the study of Boore & Toksöz (1969). They concluded (based on the investigation of partial derivatives of ellipticities and phase velocities with respect to layer parameters) that both quantities were equally sensitive to layer structure. One possible explanation for our contrasting result is that we only use the shape of the ellipticity not the absolute values. The reason for this is we believe that for ambient vibrations—owing to the presence of an unknown number of Love and body waves—absolute spectral ratios will not be a very precise measure of theRayleigh wave ellipticity. For the interpretation of the shape, however, we only have to assume that these distortions are constant as a function of frequency.

In order to compare the inversion performance based on dispersion curves and ellipticities for a well-controlled situation, we have tried to reconstruct the velocity model for a single gradient layer above half-space (Fig. 8). This model can be seen as a simplified version of the shallow part of the reference model for the Lower Rhine Embayment. The layer parameters were chosen following Ibs-von Seht & Wohlenberg (1999) for a maximum spectral ratio at 0.5 Hz. For the inversion, only the surface shear wave velocity and the layer thickness were used as free parameters while all the other parameters were kept fixed. Again, the dispersion curve allows one to reconstruct the absolute values of the velocity quite nicely while it fails to constrain the layer thickness. The models resulting from the ellipticity inversion perform less satisfactory in matching the absolute velocities and in matching the layer thicknesses. Considering the non-uniqueness of the resulting velocity models, it is

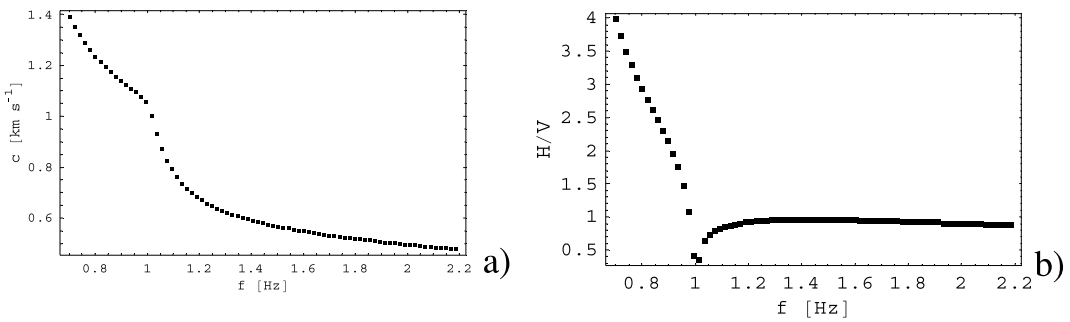

Figure 6. Dispersion curve (a) and ellipticity (b) for the reference model shown in Fig. 4(a).

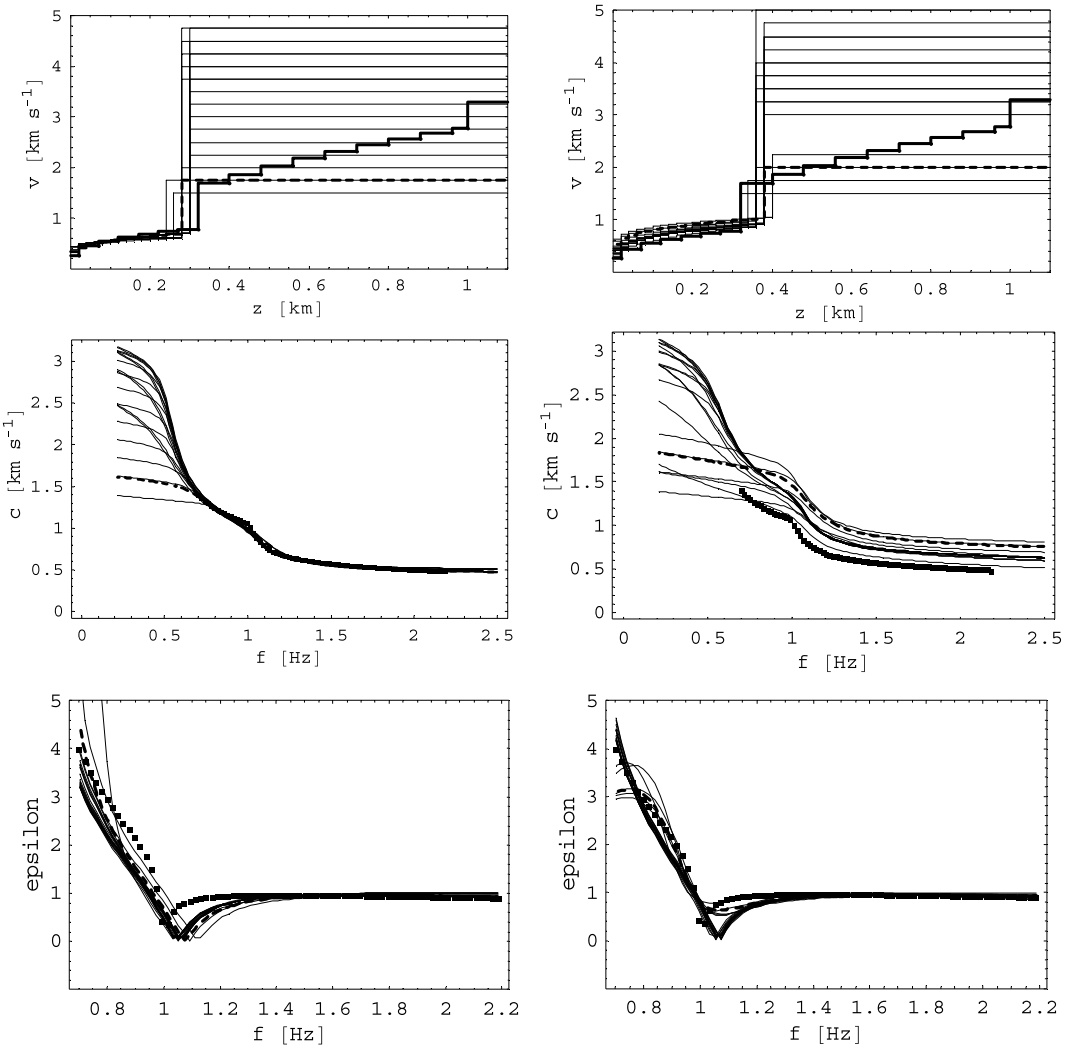

Figure 7. Inversion results for the Lower Rhine Embayment reference model. Shown from top to bottom are the 20 best-fitting velocity–depth models followed by the corresponding dispersion curves and ellipticities., respectively. The left-hand panels correspond to the minimization of the dispersion curve residuals (r_c) while the right-hand panels correspond to the minimization of the ellipticity residuals (r_{ell}). The heavy solid line and the solid squares correspond to the reference model. The heavy dashed lines show the results for the inverted model with the lowest residual.

interesting to look into the distribution of the residuals (r_c and r_{ell}) as a function of the surface velocity (v_0) and the layer thickness (d). This is displayed in Fig. 9. The absolute values of the residuals are indicated by the contour line labels. The residual plane for r_c has a clear minimum while the residual plane for r_{ell} indicates a clear tradeoff between the surface velocity and the layer thickness. The shape of the ellipticity is obviously insensitive to models for which $v_0/\mathrm{d} = \text{constant}$. This is equivalent to models for which the traveltime within the layer is constant. This can also be seen in Fig. 10, which shows the same models as in Fig. 8 only as a function of two-way traveltime (TWT) instead of depth.

We can make use of this observation by combining the dispersion curve inversion with the inversion of ellipticities. This can be done in a number of different ways, e.g. by defining and minimizing a single joint misfit function, by nested ranking of individual misfit functions, etc. The way we choose to do it here is by defining individual levels of acceptable misfits for each misfit function. Finally, we keep only those models (final accepted model set) for which all the misfit functions that we want to consider jointly fall below the predefined thresholds. Below we will refer to this approach as combined inversion. In this context it is interesting to ask which misfit functions are useful in practice. Is the shape of the ellipticity really telling us something concerning the velocity structure or is it mainly the position of the singularities that constrains the model? There are several aspects to this question. As can be seen in Figs 7–9 for the single-layer models, the shapes of the ellipticities can be very similar for significantly differing velocity models as long as the traveltime within the layer is more or less constant. Since the reciprocal four-way traveltime down to the first large impedance contrast in the generic basin model correlates well with the frequency of maximum ellipticity (Fig. 11), it seems sufficient to use only r_{ellmax} and possibly r_{ellmin} to constrain the traveltime within the single layer. From a practical point of view, one could also argue that owing to body and Love wave contributions, it will always be hard to judge in practice to what degree H/V spectral ratios obtained from ambient vibrations will actually represent Rayleigh wave ellipticities. This is especially true for the frequency range in which the shape of the ellipticities changes most, namely close to the minimum and maximum values. One way to overcome this problem is seen in the type of preprocessing suggested by Fäh *et al.* (2001). A

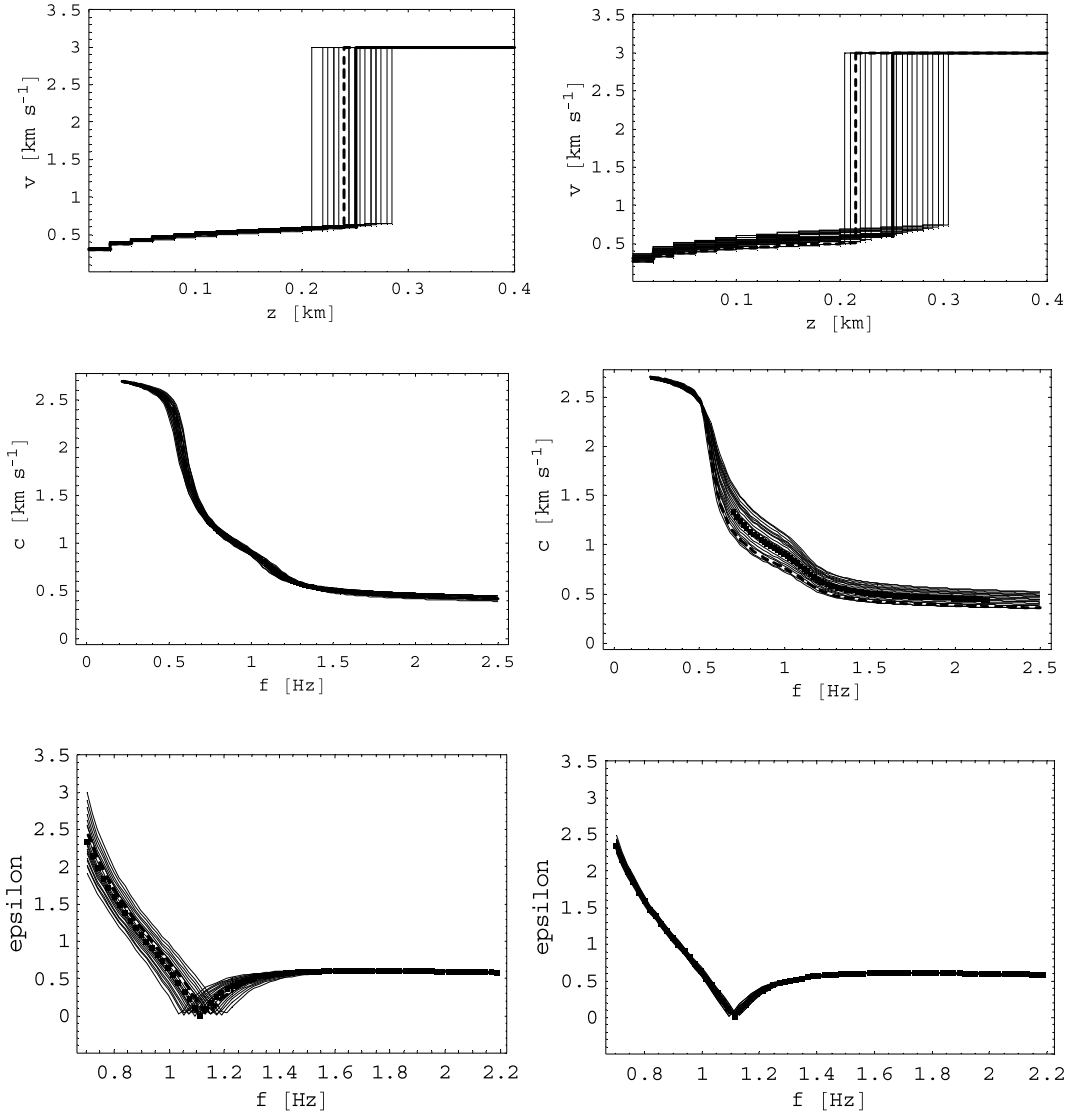

Figure 8. Inversion results for the single-layer model. Shown from top to bottom are the 20 best-fitting velocity–depth models followed by the corresponding dispersion curves and ellipticities, respectively. The left-hand panels correspond to the minimization of the dispersion curve residuals (r_c) while the right-hand panels correspond to the minimization of the ellipticity residuals (r_{ell}). The heavy solid line and the solid squares correspond to the input model. The heavy dashed lines show the results for the inverted model with the lowest residual.

further evaluation of this issue, however, is beyond the scope of this paper.

The result of the combined inversion for the single-layer model is shown in Fig. 12. It is obvious that the traveltime constraint that is caused by including r_{ellmax} as a second cost function improves the inversion considerably. The best-fitting models within the final accepted model (dashed lines in Fig. 12) essentially reproduce the input model. A similar improvement is obtained for the full Lower Rhine Embayment reference model as can be seen in Fig. 13. Here the depth to the first strong impedance contrast at roughly 300 m is fairly well recovered, although as expected the resolution for the deeper structure remains lacking.

Regarding the implications for hazard assessment it is interesting to ask how well the site amplification functions for the remaining model set matches those of the input model. This is displayed in Fig. 13. At the fundamental resonance frequency (0.5 Hz), the inverted models underestimate the site amplification by not more than 20 per cent.

3.2 Shear velocity profiles for the Cologne area

The results for the Lower Rhine Embayment reference model suggest that even with frequency band-limited data from 1 km aperture arrays, the uppermost part of the shear velocity profiles might be recoverable by a combined inversion of dispersion curves and ellipticities. We have applied this method to the data shown in Fig. 3 and Table 1. The free parameters that were inverted for are the shear wave velocity at the surface (v_0), the velocity exponent (α_s) and the layer thickness (d). Following Budny (1984), the P-wave velocity within the layer was fixed at $v_p(z) = 1470\, z^{0.057}$ (v_p in m s^{-1} for $z >$ 0 in m). For the half-space we used $v_p = 5200$ m s^{-1}, $v_s = 3000$ m s^{-1}. The densities were fixed at $\rho = 2000$ kg m^{-3} for the sediment layer and $\rho = 2700$ kg m^{-3} for the half-space, respectively. The inversion results are displayed in Figs 14–16 .

Table 2 displays the results for those models within the final accepted model space with the lowest residuals, r_{ellmax}. Considering the different techniques and also the different locations for our study

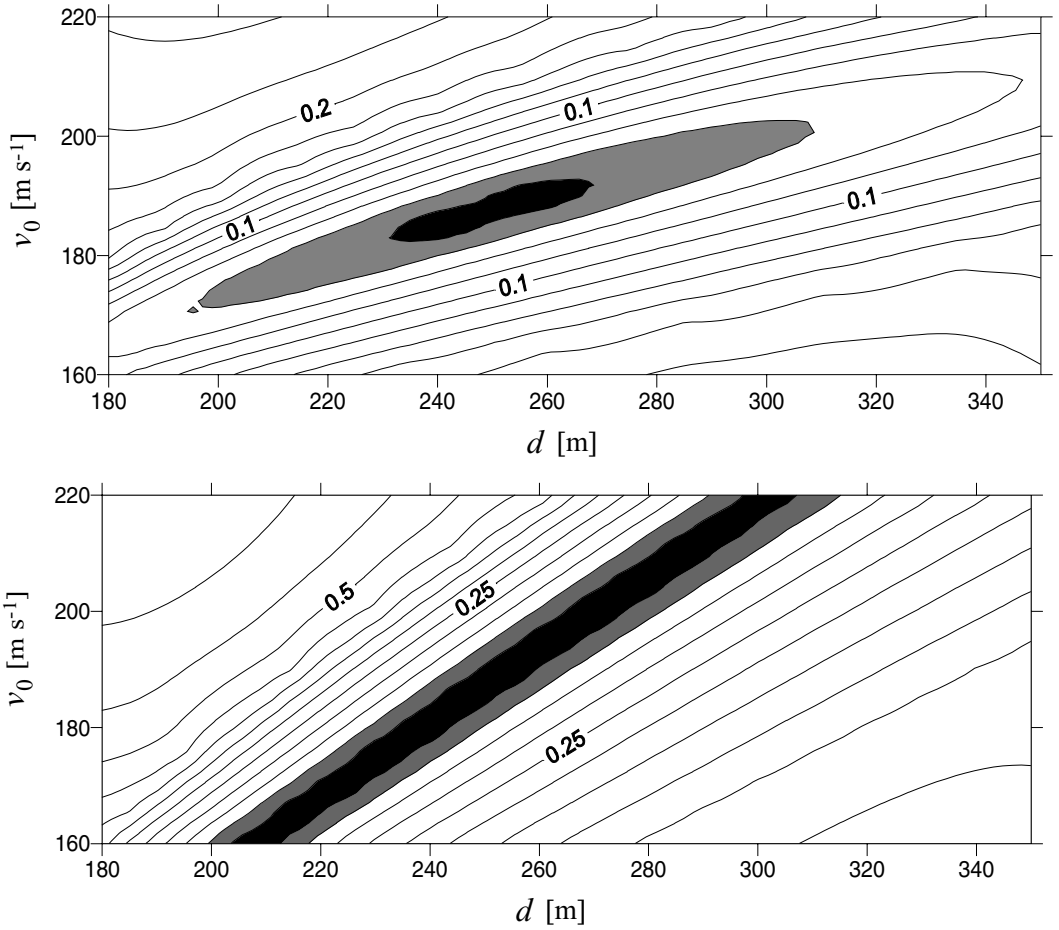

Figure 9. Distribution of the residuals (r_c and r_{ell}) as a function of the surface velocity (v_0) and layer thickness (d). The upper panel corresponds to the dispersion curve residuals (r_c) while the lower panel corresponds to the ellipticity residuals (r_{ell}).

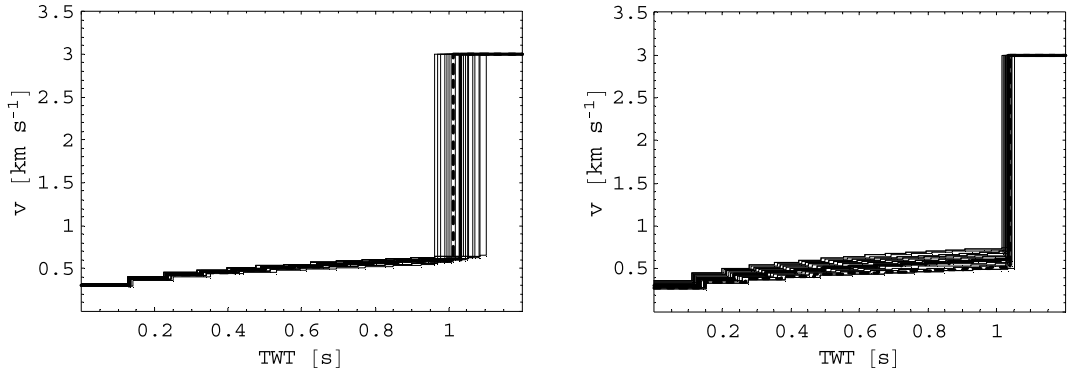

Figure 10. Inversion results for the single-layer model displayed as velocity/two-way traveltime models. The left-hand panel corresponds to the minimization of the dispersion curve residuals (r_c) while the right-hand panel corresponds to the minimization of the ellipticity residuals (r_{ell}). The heavy solid line corresponds to the input model. The heavy dashed line shows the results for the model with the lowest residual.

and the study of Budny (1984), the results are in remarkable agreement. It should also be noted that the depth to the sediment bottom at Chorweiler and Pulheim is very close, which is consistent with their spatial proximity. For all three sites the predicted site amplification factors at the fundamental frequency are of the order of 5–6 with a slightly smaller value of 5 at Lülsdorf. Since a single layer (even with a power-law depth dependence) is a very strong simplification of the true situation, these values should be taken with a pinch of salt. In order to at least partially address the question of whether deeper parts of the structure might be resolvable, we calculated an additional set of models in which we took the models given by the values in Table 2 and added a transitional layer of 100 m thickness and varying velocity between the sediments and the halfspace. Only for the Pulheim site did we see a slight indication that including such a transitional layer would reduce the residual. This is shown in Fig. 17. For Lülsdorf and Chorweiler sites, the best-fitting

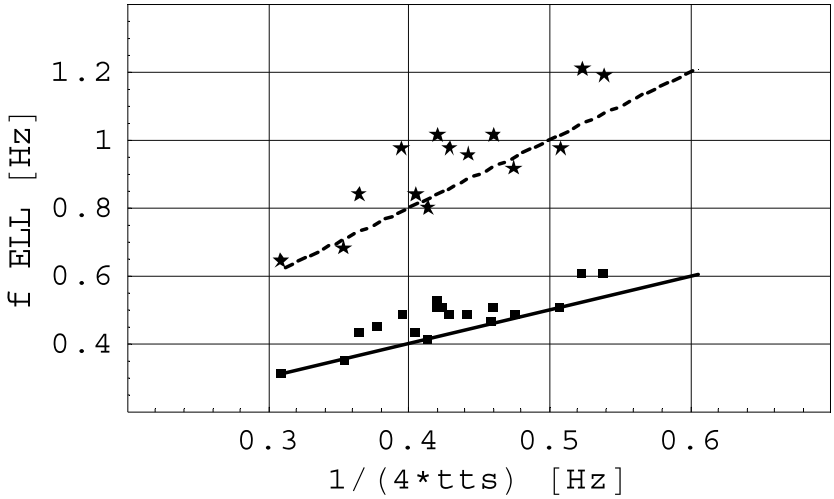

Figure 11. Frequencies of maximum (solid squares) and minimum (stars) ellipticities for the randomized basin model (Fig. 4c) plotted against the reciprocal of the four-way traveltime to the sediment–rock interface. The solid line correspond to the equation $f_{\mathrm{ellmax}} = 1/(4\ tts)$, where *tts* is the one-way traveltime and f_{ellmax} is the frequency of maximum ellipticity. The dashed line corresponds to the equation $f_{\mathrm{ellmin}} = 1/(2\ tts)$, where *tts* is the one-way traveltime and f_{ellmin} is the frequency of minimum ellipticity.

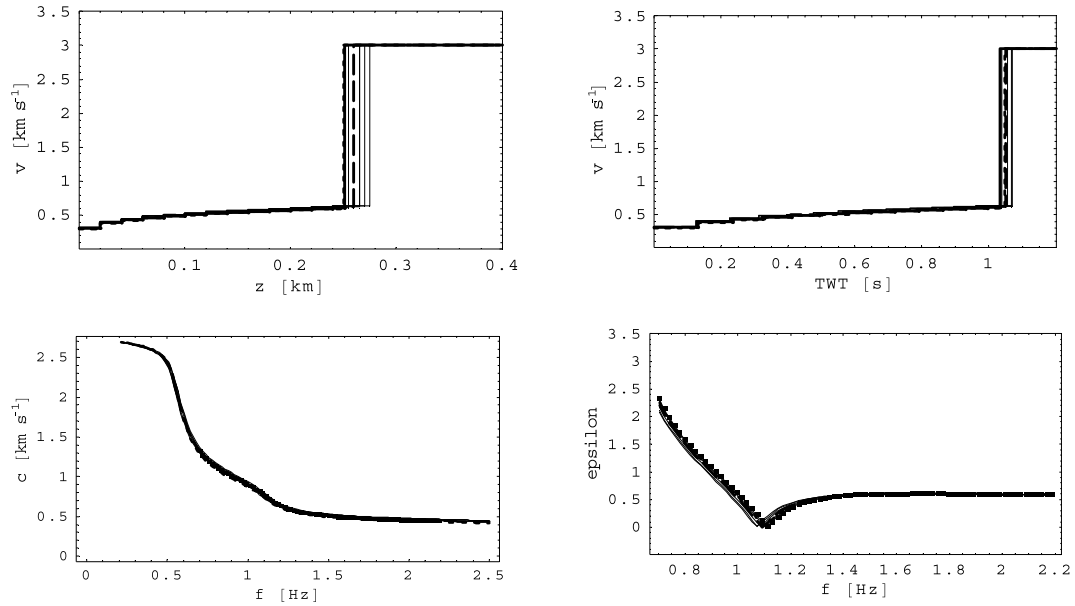

Figure 12. Combined inversion results for the single-layer model based on combining r_{c} and r_{ellmax} as described in the text. The top row shows the remaining velocity–depth models (left-hand panel) and the velocity/two-way traveltime models (right-hand panel). The bottom row shows the corresponding dispersion curves (left) and ellipticities (right). The heavy solid lines correspond to the input model. The heavy long and short dashed lines correspond to the models with the lowest r_{c} and r_{ellmax} within the final accepted model set, respectively.

model remained the same. The site amplification factors did not change much either.

4 DISCUSSION AND CONCLUSION

We have used both single-station and array methods to determine shallow shear wave velocity site profiles in the Cologne area from ambient vibration records. We assume that fundamental-mode Rayleigh waves dominate the analysed wavefield at least in the frequency range for which we observe dispersion. In order to keep the parameter space in the inversion simple we attempted to fit a single layer over the half-space model. However, owing to earlier studies of the region (Budny 1984), we assume a power-law depth dependence for sediment velocities. Both the dispersion curve and the shape of the ellipticities contain information that can be used for the inversion of the shear velocity–depth model. However, dispersion curves were found to provide stronger constraints towards the absolute values of the velocity–depth model than the ellipticities. The shape of the ellipticities was found to be subject to a strong tradeoff between the layer thickness and the average layer velocity. We have made use of this observation by combining the inversion schemes for dispersion curves and ellipticities such that the velocity–depth dependence is essentially constrained by the dispersion curves while the layer thickness is constrained by the ellipticities. Based on the tests with synthetic data believed to be representative for the Lower

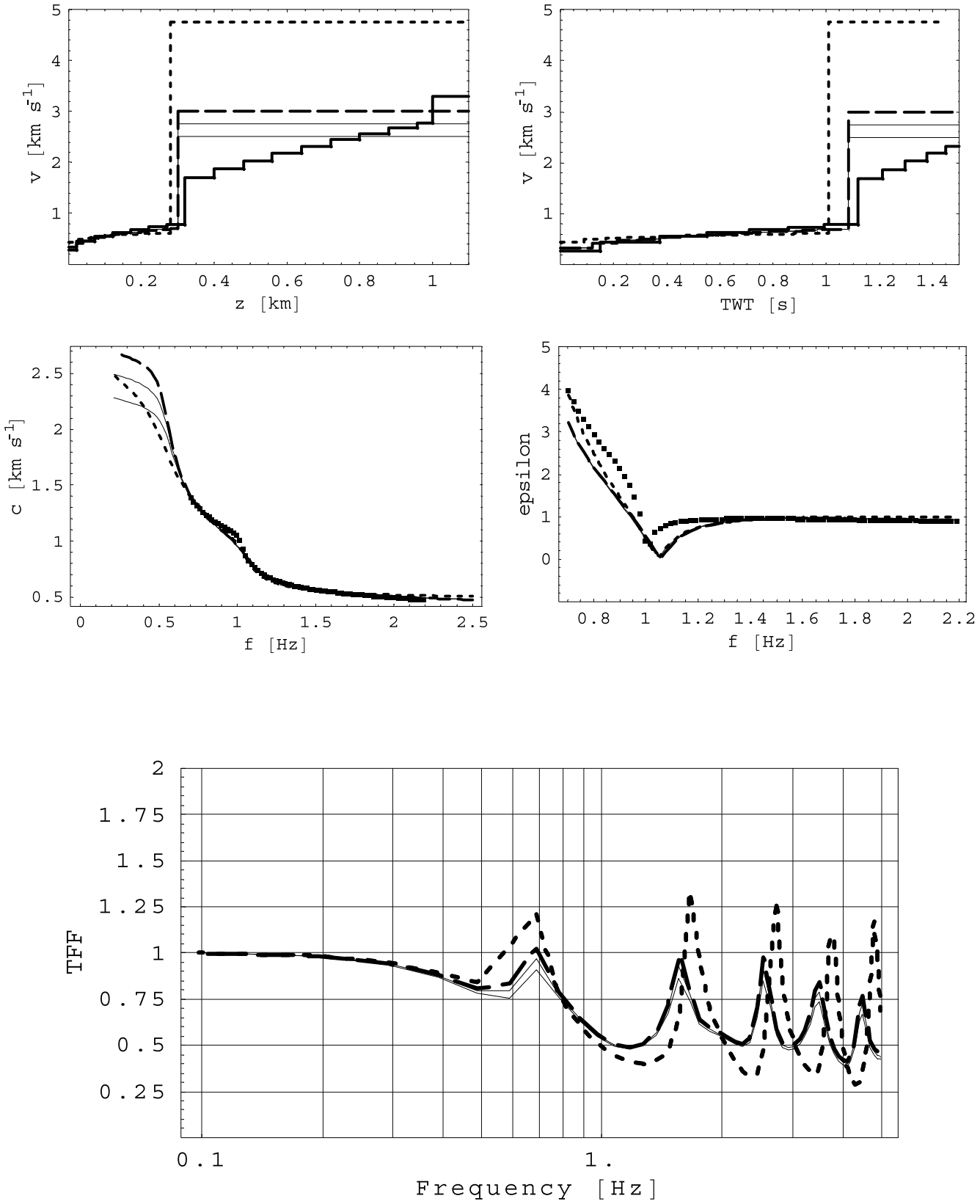

Figure 13. Combined inversion results for the Lower Rhine Embayment reference model based on combining r_c and r_{ellmax} as described in the text. The top row shows the remaining velocity–depth models (left-hand panel) and the velocity/two-way traveltime models (right-hand panel). The middle row shows the corresponding dispersion curves (left) and ellipticities (right). The heavy solid lines correspond to the input model. The heavy long and short dashed lines correspond to the models with the lowest r_c and r_{ellmax} within the final accepted model set, respectively. The bottom row shows the ratio of site amplification functions for the remaining model set with respect to the Lower Rhine Embayment reference model shown in Fig. 4(b) (a value of 1 corresponds to a perfect match).

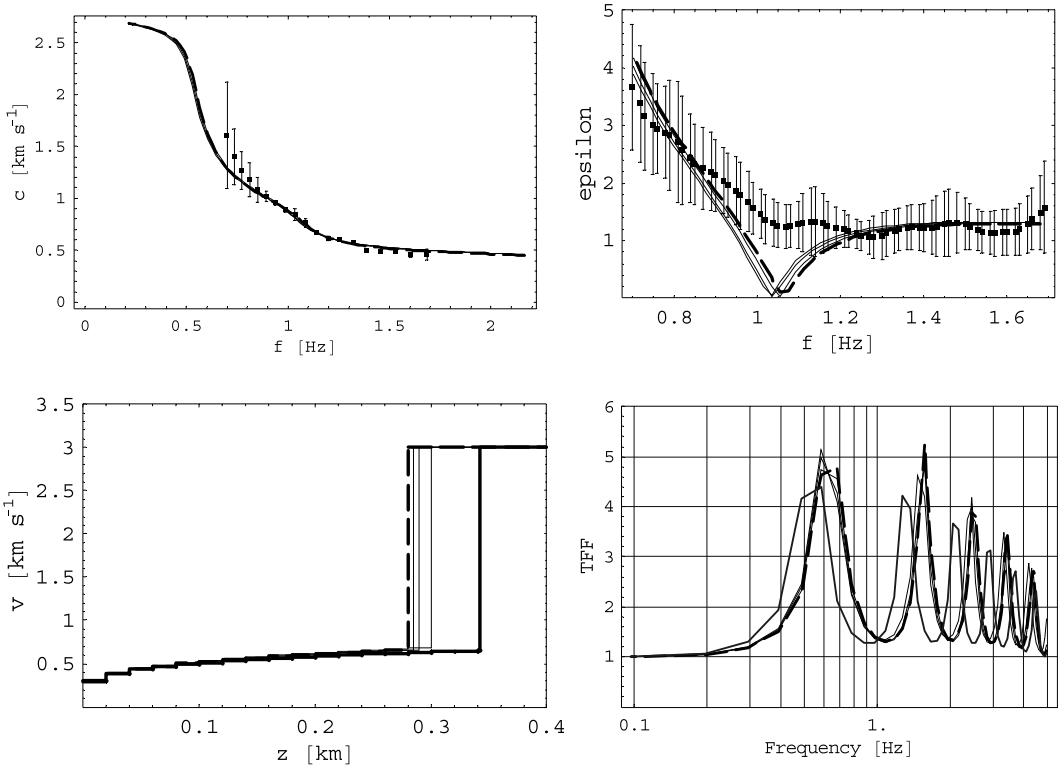

Figure 14. Combined inversion results for the Lülsdorf array site based on combining r_c and r_{ellmax} as described in the text. The top row shows the observed dispersion curves (left) and H/V spectral ratios (right). The bottom row shows the velocity–depth models obtained (left-hand panel) and the corresponding site amplification curves (right-hand panel). The heavy solid lines correspond to the model based on the shear velocities of Budny (1984) combined with the layer thickness estimate by Ibs-von Seht & Wohlenberg (1999). The heavy long and short dashed lines correspond to the models with the lowest r_c and r_{ellmax} within the final accepted model set, respectively.

Table 2. Layer parameters of the best-fitting models from the final accepted model sets. Values in parenthesis refer to the v_0 and α_s values obtained by Budny (1984) and the layer thickness according to the empirical relationship by Ibs-von Seht & Wohlenberg (1999).

Array	v_0 (m s^{-1})	α_s	d (m)
Lülsdorf	170 (188)	0.24 (0.213)	280 (342)
Chorweiler	200 (188)	0.22 (0.213)	190 (157)
Pulheim	230 (188)	0.16 (0.213)	195 (195)

Rhine Embayment, we found that we can thus reconstruct the shear wave velocity subsurface structure down to the bottom depth of the tertiary sediments at several hundreds of metres. As has been pointed out by Boore & Brown (1998), a visual comparison of velocity profiles does not allow an easy judgement of the corresponding site amplification effects. Therefore, we calculated the ratios of the corresponding *SH*-wave site amplification functions with respect to the site amplification of the reference model as suggested in a slightly different form by Boore & Brown (1998). The corresponding site amplification functions only differed by approximately 20 per cent at the fundamental resonance frequency. The application of this method to the field observations from the Cologne area resulted in models for which the shear velocity within the sediment layer both in absolute value at the surface and in depth dependence are found to be remarkably similar to the results obtained by Budny (1984) from downhole measurements. This agreement is seen as strong support for the assumption that within the frequency band investigated the vertical component records of ambient vibrations within the study area are dominated by fundamental-mode Rayleigh waves. Although the resulting models are 1-D, the resulting layer thicknesses may nevertheless be an important parameter. In the Los Angeles Basin, for example, the sediment depth has been reported to be a good proxy for the 3-D response and basin edge effects (Field 2000; Joyner 2000).

We draw some practical conclusions from the results of the present study. Velocity–depth models obtained from the inversion of H/V spectral ratios may suffer from the tradeoff between the average velocity and layer thickness and hence may not be very reliable in terms of absolute velocity–depth values. This might be especially problematic if non-exhaustive optimization schemes (e.g. simulated annealing, genetic algorithms) are employed. On the other hand, if information on the depth dependence of shear velocity is available (e.g. from dispersion curves or shallow boreholes), peak frequencies of spectral ratios were found to constrain the layer thickness quite well. Consequently, single-station and array recordings of ambient vibrations can provide complementary information regarding a reliable determination of shallow shear velocity profiles.

ACKNOWLEDGMENTS

We gratefully acknowledge the continuous technical support and the organization of the field experiments by Daniel Vollmer. We thank Georg Bissing, Sharon K. Reamer, Jürgen Mackedariz, Nebil Bayrakcioglu, Holger Gaensicke, Angela Sachse and Rita Streich, for their help with the measurements and R. B. Herrmann for providing his software. We appreciate the thoughtful reviews and

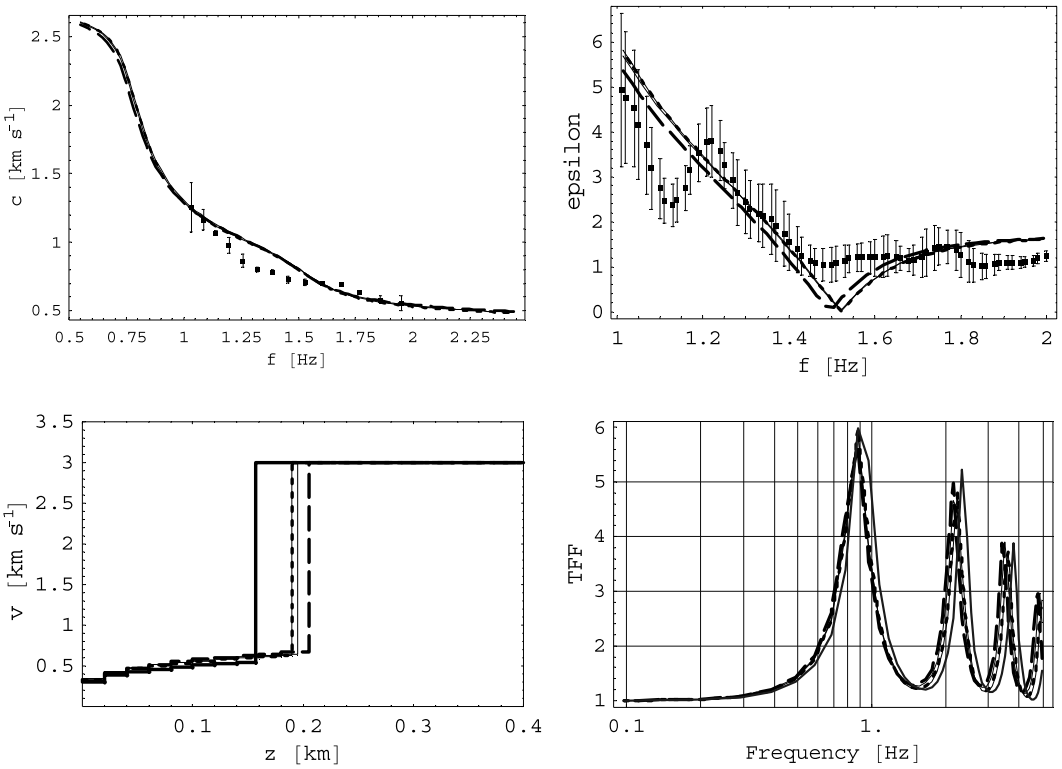

Figure 15. Combined inversion results for the array site Chorweiler based on combining r_c and r_{ellmax} as described in the text. The top row shows the observed dispersion curves (left) and H/V spectral ratios (right). The bottom row shows the velocity–depth models obtained (left-hand panel) and the corresponding site amplification curves (right-hand panel). The heavy solid lines correspond to the model based on the shear velocities of Budny (1984) combined with the layer thickness estimate by Ibs-von Seht & Wohlenberg (1999). The heavy long and short dashed lines correspond to the models with the lowest r_c and r_{ellmax} within the final accepted model set, respectively.

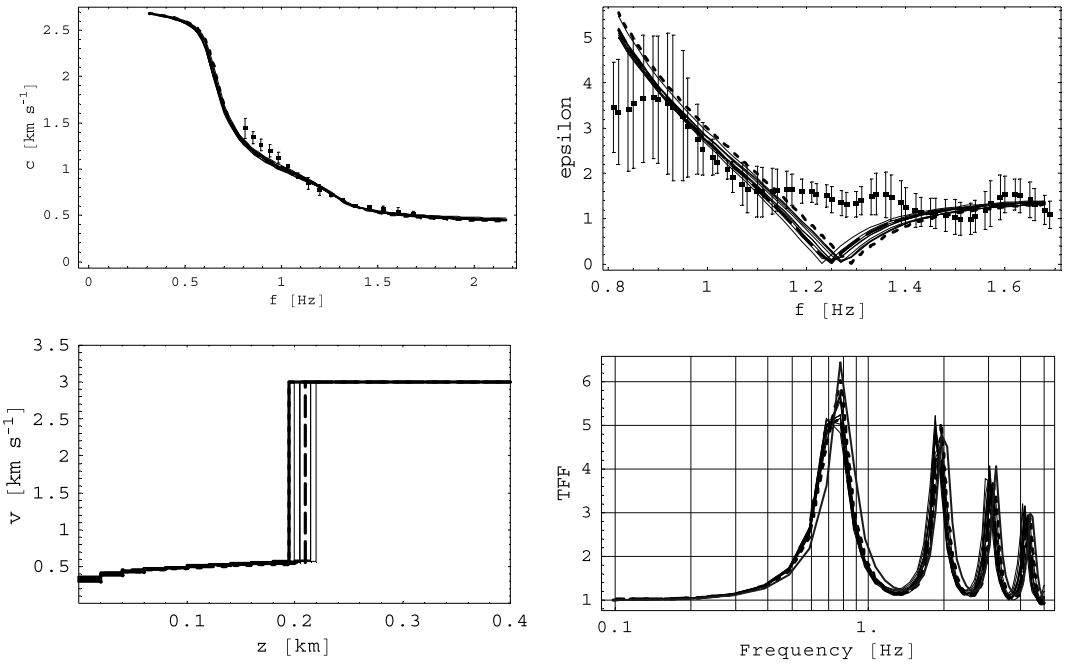

Figure 16. Combined inversion results for the Pulheim array site based on combining r_c and r_{ellmax} as described in the text. The top row shows the observed dispersion curves (left) and H/V spectral ratios (right). The bottom row shows the velocity–depth models obtained (left-hand panel) and the corresponding site amplification curves (right-hand panel). The heavy solid lines correspond to the model based on the shear velocities of Budny (1984) combined with the layer thickness estimate by Ibs-von Seht & Wohlenberg (1999). The heavy long and short dashed lines correspond to the models with the lowest r_c and r_{ellmax} within the final accepted model set, respectively.

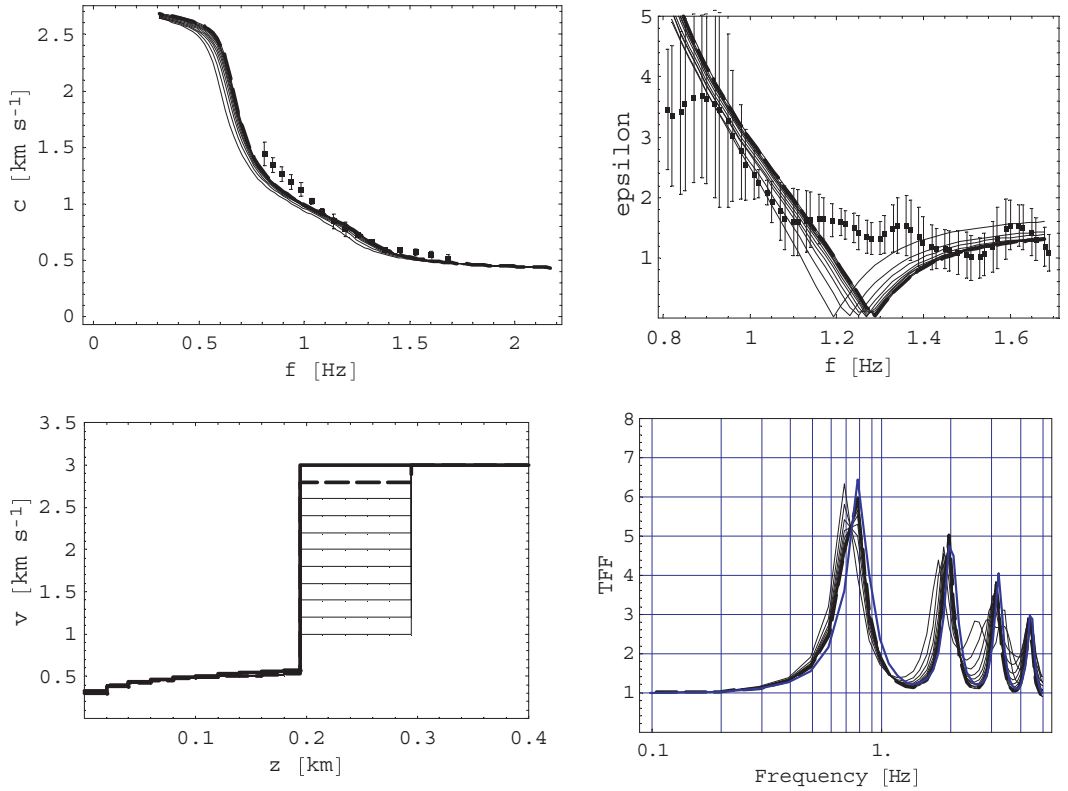

Figure 17. Effect of a transitional layer on the inversion results for the array site Pulheim. For the surface layer the model parameters were kept fixed at the values given in Table 2. An additional layer of 100 m thickness with varying shear wave velocities was included above the half-space. The top row shows the observed dispersion curves (left) and H/V spectral ratios (right). The bottom row shows the velocity–depth models (left-hand panel) and the corresponding site amplification curves (right-hand panel). The heavy solid lines correspond to the model based on the shear velocities of Budny (1984) combined with the layer thickness estimate following Ibs-von Seht & Wohlenberg (1999). The heavy dashed lines correspond to the model with the lowest residual r_c.

constructive comments by Kazuyoshi Kudo and Denis Jongmans. MO was funded by EU grant no EVG-1-CT-2000-00026.

REFERENCES

Al Yuncha, Z. & Luzón, F., 2000. On the horizontal-to-vertical spectral ratio in sedimentary basins, *Bull. seism. Soc. Am.,* **90,** 1101–1106.

Arai, H. & Tokimatsu, K., 1998. *Second International Symposium on the Effects of Surface Geology on Seismic Motion*, Yokohama, Balkerna, 2, 637–680.

Bard, P.-Y., 1998. Microtremor measurements: a tool for site effect estimation?, State-of-the-art paper, *Second International Symposium on the Effects of Surface Geology on Seismic Motion*, Yokohama, Balkerna, 3, 1251–1279.

Boore, D.M. & Brown, L.T., 1998. Comparing shear-wave velocity profiles from inversion of surface-wave phase velocities with downhole measurements: systematic differences between the CXW method and downhole measurements at six USC strong-motion sites, *Seismol. Res. Lett.,* **69,** 222–229.

Boore, D.M. & Toksöz, M.N., 1969. Rayleigh wave particle motion and crustal structure, *Bull. seism. Soc. Am.,* **59,** 331–346.

Brüstle, W. & Stange, S., 1999. Geologische Untergrundklassen zum Entwurf von Normspektren für DIN 4149 (neu), LRGB Baden-Württemberg, AZ: 3480.01/98–4764.

Budny, M., 1984. Seismische Bestimmung der bodendynamischen Kennwerte von oberflächennahen Schichten in Erdbebengebieten der niederrheinischen Bucht und ihre ingenieurseismologische Anwendung, Geologisches Institut der Universität zu KöIn, Sonderveröffentlichungen, no 57.

ESG98, 1998. *Proceedings of the Second International Symposium on the Effects of Surface Geology on Seismic Motion*, Yokohama, Balkerna, 3 volumes.

Fäh, D., Kind, F. & Giardini, D., 2001. A theoretical investigation of average H/V ratios, *Geophys. J. Int.,* **145,** 535–549.

Field, E.H., 2000. A modified ground-motion attenuation relationship for southern California that accounts for detailed site classification and a basin-depth effect, *Bull. seism. Soc. Am.,* **90,** S209–S221.

Herrmann, R.B., 1996. Computer programs in seismology, Version 3.0.

Horike, M., 1985. Inversion of phase velocity of long-period microtremors to the s-wave-velocity structure down to the basement in urbanized areas, *J. Phys. Earth*, **33,** 59–96.

Ibs-von Seht, M. & Wohlenberg, J., 1999. Microtremor measurements used to map thickness of soft sediments, *Bull. seism. Soc. Am.,* **89,** 250–259.

Ishida, H., Nozawa, T. & Niwa, M., 1998. Estimation of deep surface structure based on phase velocities and spectral ratios of long-period microtremors, *Second International Symposium on the Effects of Surface Geology on Seismic Motion*, Yokohama, Balkerna, 2, 697–704.

Joyner, W.B., 2000. Strong motion from surface waves in deep sedimentary basins, *Bull. seism. Soc. Am.,* **90,** S95–S112.

Kudo, K., 1995. Practical estimates of site response, State-of-the-Art report, *Proceedings of the Fifth International Conference on Seismic Zonation*, Nice.

Lachet, C. & Bard, P.-Y., 1994. Numerical and theoretical investigations on the possibilities and limitations of the 'Nakamura's' technique, *J. Phys. Earth*, **42,** 377–397.

Mooney, H.M. & Bolt, B.A., 1966. Dispersive characteristics of the first three Rayleigh modes for a single surface layer, *Bull. seism. Soc. Am.,* **56,** 43–67.

Miyakoshi, K., Kagawa, T. & Kinoshita, S., 1998. Estimation of geological structures under the Kobe area using the array recordings of microtrernors, *Second International Symposium on the Effects of Surface Geology on Seismic Motion,* Yokohama, Balkema, 2, 691–696.

Ohrnberger, M., 2001. Continuous automatic classification of seismic signals of volcanic origin at Mt. Merapi, Java, Indonesia, *Dissertation* University of Potsdam, p. 168.

Tazime, K., 1957. Minimum group velocity, maximum amplitude and quarter wavelength law. Love waves in doubly stratified layers, *J. Phys. Earth*, **5,** 43–50.

Tokimatsu, K., 1997. Geotechnical site characterization using surface waves, *Earthquake Geotech. Eng.*, Ishiliara (ed.), Balkerna, Rotterdam, 1333–1368.

Tokimatsu, K., Shinzawa, K. & Kuwayama, S., 1992. Use of short-period microtremors for vs profiling, *J. Geotech. Eng. ASCE,* 118, **10,** 1544–1558.

US Geological Survey, 1993. Digital elevation models, data user guide 5. Reston, Virginia, p. 50.

Yamamoto, H., 1998. An experiment for estimating *S*-wave velocity structure from phase velocities of Love and Rayleigh waves in microtrernors, *Second International Symposium on the Effects of Surface Geology on Seismic Motion*, Yokohama, Balkema, 2, 697–704.